

Investigation of Hybrid Bilayer Membranes with Neutron Reflectometry: Probing the Interactions of Melittin

S. Krueger,^{*,†} C. W. Meuse,[‡] C. F. Majkrzak,[†] J. A. Dura,[†] N. F. Berk,[†]
M. Tarek,^{†,§} and A. L. Plant[‡]

NIST Center for Neutron Research, and Biotechnology Division, National Institute of Standards and Technology, Gaithersburg, Maryland 20899; and Chemistry Department, University of Pennsylvania, Philadelphia, Pennsylvania 19103

Received August 7, 2000. In Final Form: October 31, 2000

Recent improvements in neutron reflectometry methodology have afforded enhanced sensitivity for the study of biomimetic membranes. The technique has been used to probe the interactions of the peptide toxin, melittin, with supported bilayers of phospholipid and octadecanethiol or thiahexa(ethylene oxide) alkane on gold. Improvements in instrumentation and experimental design permit neutron reflectivity measurements out to a wavevector transfer of 0.7 \AA^{-1} and down to reflectivities approaching 10^{-8} , allowing unprecedented resolution of structural details in the bilayer. The data indicate that melittin strongly perturbs the phospholipid headgroup region and also affects the alkane chain region of the bilayer. There is no evidence for hydration of the ethylene oxide spacer region between the gold and alkane regions of the thiahexa(ethylene oxide) alkane/phospholipid bilayer, but a distinct shift of up to 3 \AA in the apparent location of the interface between the alkane and phospholipid regions is observed. This work shows that the neutron reflectometry technique is now sensitive to small changes in the reflected intensities, and these small changes can result in significant contributions to the resultant scattering length density profiles.

Introduction

A supported lipid bilayer consisting of a leaflet of alkanethiol and a leaflet of phospholipid has many potential advantages as a biomimetic model membrane. The sulfur of alkanethiols interacts strongly with gold and other metals, and van der Waals interactions between alkane chains drive alkanethiols into a stable, hydrophobic monolayer at a metal surface.¹ A hybrid bilayer is formed by the addition of phospholipid molecules onto this layer, either from vesicles in solution or from a monolayer of lipid at the air–water interface. Compared to other planar lipid systems, hybrid bilayer membranes (HBMs) present an opportunity for constructing a rugged, supported model system that is also biomimetic. However, this combination of characteristics presents challenges to organic synthesis, bilayer fabrication, and analytical methods. Since measurements can be made in contact with aqueous solution, neutron reflectometry studies can provide unique structural information about HBMs, which can aid in the fabrication of better biomimetic matrixes. Furthermore, hydrogenated components can be distinguished from deuterated components, making it possible to characterize the interface between the two monolayers in the HBM, provided that one contains deuterated lipid, and to detect changes in lipid structure due to the presence of membrane-active peptides and protein. This work describes the first in a series of experiments aimed at using improved neutron reflectometry experimental methods to characterize HBMs and their interactions with small peptides and membrane proteins in an effort to engineer more biomimetic HBM matrixes.

While X-ray and neutron diffraction of multilayered samples has historically been a critical source of high-resolution structural data of model biological membranes, neutron reflectometry has provided unique data to the study of single lipid bilayer membranes in contact with bulk water.^{2–6} HBMs, in particular, are well suited for neutron reflectometry measurements, since they are relatively rugged structures that are stable over the long times required for data collection and since the bilayer forms over 100% of the large sample surface that is probed. Previous neutron reflectometry experiments on octadecanethiol/DPPC HBMs in both the gel and liquid crystalline phases⁶ showed that the thickness of the DPPC acyl chain region and the area per lipid molecule agreed reasonably well with values obtained from multilayer systems of DPPC bilayers using X-ray diffraction^{7–10} and from simulations of DPPC bilayers.^{11,12} While this earlier study did provide structural information on single HBM bilayers in solution, data could only be obtained out to $Q = 0.25 \text{ \AA}^{-1}$ due to limitations in the instrumentation and sample environment. This work describes recent improvements in neutron reflectometry measurement and data analysis capabilities and their application to the study

[†] NIST Center for Neutron Research, National Institute of Standards and Technology.

[‡] Biotechnology Division, National Institute of Standards and Technology.

[§] University of Pennsylvania.

(1) Nuzzo, R. G.; Fusco, F. A.; Allara, D. L. *J. Am. Chem. Soc.* **1987**, *109*, 2358.

(2) Reinl, H.; Brumm, T.; Bayerl, T. M. *Biophys. J.* **1992**, *61*, 1025.

(3) Johnson, S. J.; Bayerl, T. M.; McDermott, D. C.; Adam, G. W.; Rennie, A. R.; Thomas, R. K.; Sackmann, E. *Biophys. J.* **1991**, *59*, 289.

(4) Koenig, B. W.; Krueger, S.; Orts, W. J.; Majkrzak, C. F.; Berk, N. F.; Silverton, J. V.; Gawrisch, K. *Langmuir* **1996**, *12*, 1343.

(5) Krueger, S.; Ankner, J. F.; Satija, S. K.; Majkrzak, C. F.; Gurley, D.; Colombini, M. *Langmuir* **1995**, *11*, 3218.

(6) Meuse, C. W.; Krueger, S.; Majkrzak, C. F.; Dura, J. A.; Fu, J.; Connor, J. T.; Plant, A. L. *Biophys. J.* **1998**, *74*, 1388.

(7) Nagle, J. F.; Wiener, M. C. *Biochim. Biophys. Acta* **1988**, *942*, 1.

(8) Wiener, M. C.; Suter, R. M.; Nagle, J. F. *Biophys. J.* **1989**, *55*, 315.

(9) Sun, W.-J.; Suter, R. M.; Knewton, M. A.; Worthington, C. R.; Tristram-Nagle, S.; Zhang, R.; Nagle, J. F. *Phys. Rev. E* **1994**, *49*, 4665.

(10) Nagle, J. F.; Zhang, R.; Tristram-Nagle, S.; Sun, W.-J.; Petrache, H. I.; Suter, R. M. *Biophys. J.* **1996**, *70*, 1419.

(11) Tu, K.; Tobias, D.; Klein, M. L. *Biophys. J.* **1995**, *69*, 2558.

(12) Tu, K.; Tobias, D.; Blasie, J. K.; Klein, M. L. *Biophys. J.* **1996**, *70*, 595.

of proteins in fully hydrated single-bilayer biomimetic membranes.

Detailed structural studies of alkanethiol/phospholipid hybrid bilayer model membranes have been performed in our laboratory by electrochemistry,¹³ surface plasmon resonance,¹⁴ and reflection-absorption infrared spectroscopy.^{6,15} The gold support can serve as an electrode, thereby providing a new tool for studying structural and functional characteristics of membranes and proteins associated with them. A number of groups have demonstrated the reconstitution of functional proteins into supported tethered model membranes.¹⁶ Melittin, in particular, has been studied extensively as a model peptide for antibiotics and for membrane proteins.¹⁷ Different studies have provided conflicting data, leading to varying conclusions about its mechanism of action and location and orientation in the bilayer. Red blood cells lyse on exposure to melittin.^{18,19} It has been demonstrated¹⁹ that the cells swell initially, which is consistent with an increase in permeability of Na⁺ and K⁺ induced by the formation of melittin pores in the membrane. On the basis of such data, the effect of melittin has been attributed to the formation of oligomeric (tetrameric) pores,²⁰ but some data also suggest a role for monomeric melittin.²¹ Previous electrochemistry experiments performed in our laboratory indicated that the addition of a solution containing melittin to HBMs results in an increase in the current which can pass through this otherwise insulating bilayer.^{13,22} However, a more recent electrochemistry study suggests that this observation could be due to simple electrostatic effects.²³

Different orientations for melittin in bilayers have been reported for different conditions of pH, lipid headgroup charge, and hydration of the membrane. Even when pH and headgroup are kept constant, it has been reported that melittin lies parallel to the alkyl chains^{24–27} or confined to the headgroup of membranes^{27–30} depending on the hydration of the bilayer or multilayer. Furthermore, Tosteson et al.³¹ reported that, at low concentrations, melittin is initially associated with the lipid headgroup and oriented perpendicular to the alkane chains until the application of a positive potential on the cis side of the membrane results in melittin insertion and reorientation parallel to the lipid alkane chains. Since neutron reflectometry experiments can potentially address these im-

portant issues, melittin was chosen as the model membrane-active peptide in these initial experiments.

Because of interest in eventually using HBMs for reconstitution of active membrane proteins, an alternative tethering molecule, thiahexa(ethylene oxide) alkane (THEO-C₁₈), was synthesized.³² THEO-C₁₈ contains ethylene oxide moieties that separate the tethering sulfur group from the alkane chain. Like alkanethiols, this molecule associates with the gold support via its sulfur moiety. Ethylene oxide groups associated with alkanethiols have been reported to be hydrated and disordered. It was anticipated that this molecule would assemble into a relatively disordered monolayer, thus providing the THEO-C₁₈ leaflet with a biomimetic character. Surprisingly, initial FTIR spectroscopy measurements of monolayers of THEO-C₁₈ in air³² revealed a high degree of molecular order. Neutron reflectometry, however, allowed examination of the structure of a monolayer of THEO-C₁₈ in an HBM and in contact with water. Therefore, these experiments provided the potential for observing a very different structure in a very different, and more biologically relevant, environment.

Thus, the neutron reflectometry experiments reported here were designed to answer the important question of whether the ethylene oxide moieties are hydrated when the HBM is in contact with water and to probe the structural changes that occur when the HBM interacts with melittin. The results obtained from the structural studies demonstrate the sensitivity of the neutron reflectometry technique to changes in bilayer structure in the presence of membrane-active proteins and peptides.

Materials and Methods⁴⁸

Sample Preparation. The samples were prepared in a three-step process that first involved coating a single-crystal silicon (Si) substrate with a thin (50 Å thick) gold layer. To avoid contamination of the gold surface, the gold-coated silicon wafers were placed in an alkanethiol solution immediately after the gold deposition, allowing an alkanethiol monolayer to self-assemble on the gold surface. The final step involved the deposition of a phospholipid layer onto the alkanethiol layer using a modified Langmuir-Blodgett method described below. This procedure resulted in the formation of an HBM in air, which was subsequently rehydrated with either D₂O solution or D₂O buffer containing melittin. Details of the entire procedure follow.

The gold coating on Si was prepared using a Millatron DBS Model 3424 for thermal evaporation and ion milling, as reported previously,³³ and was deposited over 15–20 Å barrier films of chromium. The THEO-C₁₈ monolayers (HS(C₂H₄O)₆(CH₂)₁₇CH₃) and the first of two octadecanethiol (HS(CH₂)₁₇CH₃) (Aldrich, 97%) monolayers (sample no. 1) were prepared by immersing the metal substrates in 1 mM thiol solutions of 200 proof ethanol (Warner Graham Co., Cockeysville, MD) for a minimum of 12 h. To avoid the formation of multilayers,³⁴ a separate procedure was used for the second octadecanethiol monolayer (sample no. 2). This layer was prepared by immersing the substrate in 0.2 mM octadecanethiol in hexadecane (Aldrich) for 1 min. The substrate was rinsed by placing it in a series of solvents and was blown dry with a stream of nitrogen gas after each immersion. The order was

(13) Plant, A. L.; Gueguetchkeri, M.; Yap, W. *Biophys. J.* **1994**, *67*, 1126.

(14) Hubbard, J. B.; Silin, V.; Plant, A. L. *Biophys. Chem.* **1998**, *75*, 163.

(15) Meuse, C. W.; Niaura, G.; Lewis, M. L.; Plant, A. L. *Langmuir* **1998**, *14*, 1604.

(16) Plant, A. L. *Langmuir* **1999**, *15*, 5128.

(17) Dempsey, C. E. *Biochim. Biophys. Acta* **1990**, *1031*, 143.

(18) Hider, R. C.; Khader, F.; Tatham, A. S. *Biochim. Biophys. Acta* **1983**, *728*, 206.

(19) Tosteson, M. T.; Holmes, S. J.; Razin, M.; Tosteson, D. C. *J. Membr. Biol.* **1985**, *87*, 35.

(20) Tosteson, M. T.; Tosteson, D. C. *Biophys. J.* **1981**, *36*, 109.

(21) Benachir, T.; Lafleur, M. *BBA-Biomembranes* **1995**, *1235*, 452.

(22) Plant, A. L. *Langmuir* **1993**, *9*, 2764.

(23) Brevnov, D. A.; Finklea, H. O. *Langmuir* **2000**, *16*, 5973.

(24) Vogel, H.; Jahng, F.; Hoffman, V.; Stumpel, J. *Biochim. Biophys. Acta* **1983**, *733*, 201.

(25) Vogel, H. *Biochemistry* **1987**, *26*, 4562.

(26) Brauner, J. W.; Mendelsohn, R.; Prendergast, F. G. *Biochemistry* **1987**, *26*, 8151.

(27) Frey, S.; Tamm, L. K. *Biophys. J.* **1991**, *60*, 922.

(28) Stanislawski, B.; Ruterjans, H. *Eur. Biophys. J. Biophys.* **1987**, *15*, 1.

(29) Altenbach, C.; Hubbell, W. L. *Proteins* **1988**, *3*, 230.

(30) Altenbach, C.; Flitsch, S. L.; Khorana, H. G.; Hubbell, W. L. *Biochemistry* **1989**, *28*, 7806.

(31) Tosteson, M. T.; Alvarez, O.; Hubbell, W.; Bieganski, R. M.; Altenbach, C.; Caporales, L. H.; Levy, J. J.; Nutt, R. E.; Rosenblatt, M.; Tosteson, D. C. *Biophys. J.* **1990**, *58*, 1367.

(32) Vanderah, D. J.; Meuse, C. W.; Silin, V.; Plant, A. L. *Langmuir* **1998**, *14*, 6916.

(33) Pedulla, J.; Deslattes, R. D. In *X-ray/EUV Optics*; Hoover, R. B., Walker, A. B. C., Eds.; *Proc. SPIE* **1993**, *2011*, 299.

(34) Woodward, J. T.; Walker, M. L.; Meuse, C. W.; Vanderah, D. J.; Proirier, G. E.; Plant, A. L. *Langmuir*, in press.

hexane for 5 min, ethanol for 5 min, and deionized water for 10 min. This procedure resulted in an ellipsometry film thickness of 1.8 nm (M-44 spectroscopic ellipsometer, J. A. Woollam Co., Lincoln, NE) using parameters reported previously.⁶ The phospholipid used in these studies was d₅₄-dimyristoyl phosphatidylcholine (dDMPC) (Avanti Polar Lipids, Alabaster, AL).

Dry octadecanethiol or THEO-C₁₈ monolayers were produced on the hydrophobic gold surfaces using a procedure published previously.⁶ Lipid is spread at the air-water interface of a Nima 2011 Langmuir trough (Coventry, England). The barriers are controlled to produce a surface pressure of 48 mN m⁻¹. The substrate is positioned parallel to the surface and lowered until it just makes contact with the surface of the trough containing the lipid. When the substrate is raised, the surface tension of the water prevents the separation of the sample surface and the water at all points simultaneously. The surface curves back under the sample covering the substrate with two lipid layers sandwiching a water layer. The measured transfer ratio is 200% ± 4%. If the water is allowed to dry either under ambient conditions or in a stream of nitrogen, the second lipid layer comes to rest on the first. To remove the second outer layer of lipid, the wet sample is blotted onto a stack of filter paper. This blotting removes the layer of water from the entire surface and brings one layer of lipid with it.

The dry bilayers were rehydrated during assembly of the neutron reflectometry cell. The surface of the cell that faces the bilayer consisted of a second silicon wafer in which the center had been etched out to a depth of 15–20 μm. To etch the wafer, an outer ring approximately 15 mm thick was masked on the second wafer using an etch-stop wax dissolved in tetrachloroethylene. The wafer was then etched in a solution of 57% nitric acid, 18% hydrofluoric acid, and 25% acetic acid for an experimentally determined amount of time. The etch-stop wax was then removed. The etched cavity was overfilled with an appropriate aqueous solution, and the first silicon wafer containing the sample was then placed face down on the second in one continuous motion to trap the water layer between the wafers.

Melittin (86 wt %) was purchased from Sigma and used without further purification. Solutions were prepared in 20 mM Tris, 150 mM NaCl, pH 7.2, and contained 5 mM EDTA to block any contaminating phospholipase activity. The concentration of melittin used for the neutron reflectometry experiments was nominally 4 μM, assuming an extinction coefficient³⁵ at 280 nm of 5570 M⁻¹ cm⁻¹ and a molecular weight of 2847. This concentration in solution was chosen because it corresponds to approximately 50 lipid molecules per melittin molecule in the HBMs.

HBM samples were rehydrated in the presence of melittin in the same way as described above, except that the melittin solution was used in place of the water in the etched silicon wafer. Before melittin solution was added to the THEO-C₁₈/dDMPC HBM samples, the dDMPC layer was removed from the surface by rinsing with 2-propanol, followed by water, and a new layer of phospholipid was redeposited from the Langmuir trough as described above.

The same gold-coated silicon substrate was used for all octadecanethiol/dDMPC and THEO-C₁₈ HBMs. Thiols were removed using a Boekel UV cleaner Model B5500 (Boekel Industries, Feasterville, PA). Two 10-min cleaning cycles were performed, with ethanol rinses after each. Details are given in ref 34.

Neutron Reflectivity Measurements. Measurements were performed at the NG1 reflectometer at the National Institute of Standards and Technology (NIST) Center for Neutron Research (NCNR). The specular reflectivity was measured as a function of incident angle, θ , using standard θ - 2θ scans. The neutron wavelength, λ , was 4.75 Å with a wavelength spread, $\Delta\lambda/\lambda$, of 0.01. The neutron beam was collimated by two slits before the sample, which are opened in proportion to the incident angle throughout the scan to illuminate the same sample area at all incident angles. For the HBM measurements, the beam height was fixed at 2.5 cm and the slits were opened so as to continuously accommodate a 5 cm sample length. Two slits positioned after the sample are opened with respect to the front slits such that they always accept all of the specular scattering from the sample.

Two different off-specular “background” scans were made using the same 2θ values, but with θ offset to $\theta + 0.5\theta$ in one case and to $\theta - 0.15\theta$ in the other. These parameters were determined by performing “rocking curves”, where 2θ is held constant and θ is varied, at several different 2θ values in order to determine the background level on both sides of the peak θ value. The two background scans, made on either side of the peak θ value, were then averaged to give the interpolated background at the peak θ position. This was found to be identical to fitting the two background points on either side of the specular peak to a straight line and then extrapolating to the peak θ position. The averaged background scan was then subtracted from the specular scan.

The data were placed on an absolute scale by dividing out the intensity differences due to the opening of the front slits. This was accomplished by performing a “slit” scan, in which the front and back slits are opened exactly as they are during the θ - 2θ scan, but with $\theta = 2\theta = 0.0$ for all points. Then, the background-corrected specular scan is divided by the slit scan, point-by-point, to obtain the specular reflectivity on an absolute scale. Finally, the data were written as a function of the wavevector transfer, Q , at each 2θ value using the definition $Q = 4\pi \sin(\theta)/\lambda$.

X-ray Reflectivity Measurements. Prior to the neutron reflectivity measurements, X-ray reflectivity measurements were performed at the NCNR on the gold-coated substrate in order to obtain a scattering length density profile for the chromium and gold layers. Cu K α X-rays (1.54 Å) were incident on the substrate from air. The X-ray beam was collimated with two slits before the sample (0.3 and 0.05 mm) and two slits after the sample (0.2 and 0.1 mm). The specular reflectivity was measured as a function of incident angle, θ , using standard θ - 2θ scans. Two different off-specular “background” scans were made using the same 2θ values, but with θ offset on either side of the peak θ value. The background scans were averaged to give the correct background at the peak θ position. Absorption from the sample was considered and found to have a negligible effect on the data. This is not surprising, since the thickness of the gold layer is only 50 Å. The data were then rescaled so that the reflected intensity at the critical angle of the gold ($\theta = 0.3^\circ$) was equal to 1.0.

Sample Environment for Neutron Reflectivity Experiments. Previous neutron reflectivity measurements of HBMs⁶ indicated that the major source of background scattering comes from the solution in contact with the HBM. Additional measurements of silicon oxide films on silicon substrates at the NG1 reflectometer³⁶ indicated that two other significant sources of background scattering are due to scattering from air and from the

(35) Quay, S. C.; Condie, C. C. *Biochemistry* **1993**, *22*, 695.

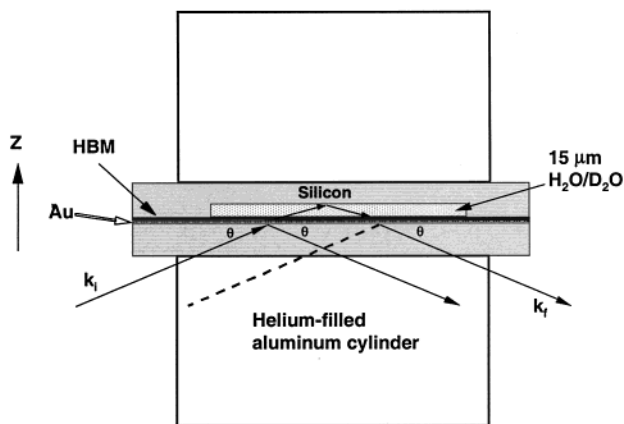


Figure 1. Top-view drawing of the neutron reflectivity sample environment for the measurement of single hybrid bilayer membranes in contact with aqueous solution.

silicon substrate itself, which had served as the incident medium for the HBM experiments. To reduce the amount of background scattering from these sources, a new sample environment and experimental method were designed.

A schematic of the new sample environment, as viewed from the top, is shown in Figure 1. Thin (0.5 mm) silicon substrates were used in order to reduce the background scattering from the silicon itself. The HBM was assembled on the substrate that is coated with a 50 Å gold film on top of a 15–20 Å chromium adhesion layer. The opposite thin silicon substrate contains a cylindrical etched region which serves as the water reservoir. The diameter of the reservoir is approximately 6.5 cm, but the thickness is restricted to 15–20 μm, to reduce the background scattering due to the solution. For the HBM experiments, the reservoir is filled with D₂O, to further minimize the solution scattering (the isotropic, incoherent scattering from hydrogen in H₂O having the largest cross-section) and enhance the signal-to-noise ratio. The entire silicon wafer assembly is placed between two helium-filled aluminum cylinders, to eliminate air scattering. Thus, except at the lowest incident angles, θ , the incident and exit media are essentially helium gas, rather than silicon or air. The entire sample environment in Figure 1 was pressed together between two aluminum blocks (not shown) which can be connected to a circulating bath for temperature control. The temperature of the silicon–HBM–D₂O–silicon sandwich was kept at 28–30 °C during the experiment, so that the dDMPC monolayer was in the fluid liquid-crystalline phase. Independent total internal reflection FTIR measurements of HBMs in water confirm that, at room temperature of approximately 24 °C, dDMPC is in a disordered state (Meuse et al., unpublished data).

To avoid refraction effects present when the beam is incident on the thin silicon substrate at low angles, measurements below $Q = 0.1 \text{ \AA}^{-1}$ are made with an additional, thick (2 cm) silicon substrate inserted between the incident silicon substrate and the helium-filled cylinder. The thick substrate is removed for measurements above this Q value. Beyond $Q = 0.05 \text{ \AA}^{-1}$, data taken with or without the thick silicon substrate present are identical to within the accuracy of the measurements. Using this new experimental setup, data were obtained out to a maximum Q value of $Q = 0.7 \text{ \AA}^{-1}$ and down to almost 10^{-8} in reflected intensity.

Scattering Length Density Profiles. Neutron scattering length density (SLD) depth profiles along the z

direction, perpendicular to the bilayer surface, were obtained from the data using the “model-independent” fitting program, PBS,³⁷ developed at the NCR. This method uses parametric B-splines to describe the SLD as a function of z . Input parameters are the SLD values of the silicon substrate and the D₂O solution, and the total thickness of the sample, including the chromium and gold layers. Unlike a model-dependent approach, no a priori knowledge of the SLD profile is necessary. A special version of PBS, which explicitly takes the scattering from the back silicon substrate into account, was written for the analysis of the HBM data. A test of the suitability of the PBS program is in Appendix A.

Several PBS fits were made for each reflected intensity versus the Q data set to obtain a family of SLD profile curves that fit the reflectivity data equally well. To judge the goodness of fit, the PBS program calculates a discrepancy ratio³⁷ (> 1.0), which is the average of the ratios between the theory and the data at each Q value. The closer the ratio is to 1.0, the better the fit to the data. In practice, it is difficult to achieve ratios smaller than 1.1 for data such as those obtained from the HBMs. In this case, fits to the data were considered “equally good” if the reported ratio was between 1.5 and 2.0.

During the PBS fits, the chromium and gold layer portions of the SLD profile were constrained to have a shape corresponding to that of the best-fit profile obtained from the X-ray measurements on the substrate alone, with the SLD values adjusted to their neutron equivalents. This can be described as a “loose” constraint, since the SLD profile in the chromium and gold regions will change by relatively small amounts during the fitting process, while the rest of the profile changes to a much greater extent. If, at some point, the chromium and gold region changes significantly from the original shape, then the fit can be restarted, replacing the SLD profile in the chromium and gold regions only with the original profile. This procedure is continued until a suitable fit to the reflectivity data is obtained over the entire measured Q -range.

Results and Discussion

In this study, neutron reflectivity curves were obtained from HBMs composed of octadecanethiol/DMPC in the presence of melittin, and HBMs composed of thiahexa-(ethylene oxide) alkane (THEO-C₁₈)/DMPC in the absence and presence of melittin. The octadecanethiol or THEO-C₁₈ layers were hydrogenated, and the DMPC was deuterated (dDMPC). The use of different isotopes provides a large change in neutron SLD between the alkane chain (CH₂) and the dDMPC acyl chain (CD₂) regions, while still maintaining a reasonable difference in SLD between the dDMPC acyl chain and lipid headgroup regions. This allowed assessment of each leaflet of the bilayer independently. DMPC was chosen, rather than DPPC, so that the lipid could be measured in the liquid crystalline phase at a temperature of 28–30 °C, much closer to room temperature, which reduced problems of liquid evaporating from the sample cell during the measurement. These changes in the sample, along with the improvements in the sample environment outlined previously, allowed for much better resolution of the individual acyl chain regions and the lipid headgroup region than had been possible in previous measurements.⁶

Gold-Coated Silicon Substrate. The results of the X-ray reflectivity measurements of the gold-coated silicon substrate provided independent data for this portion of the HBM sample, and were used to assist neutron data

(36) Dura, J. A.; Richter, C. A.; Majkrzak, C. F.; Nguyen, N. V. *Appl. Phys. Lett.* **1998**, *73*, 2131.

(37) Berk, N. F.; Majkrzak, C. F. *Phys. Rev. B* **1995**, *51*, 11296.

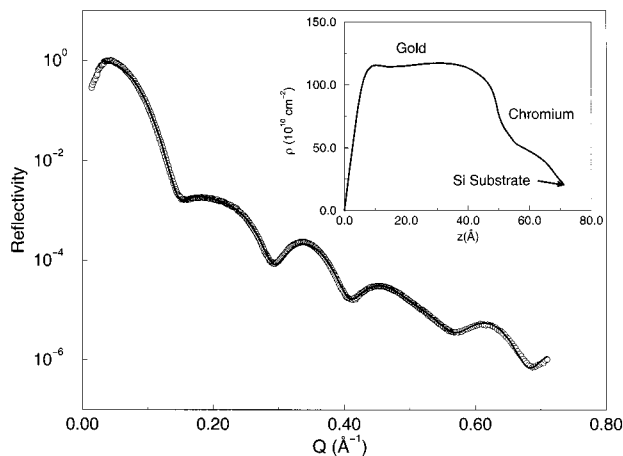


Figure 2. X-ray reflectivity data from the gold-coated silicon substrate (○), along with a representative PBS fit to the data (—). The inset shows the scattering length density profile corresponding to the PBS fit.

fitting. The data taken for the gold-coated substrate that was used for all the HBM samples are shown in Figure 2, along with one of the fits obtained using the PBS program. The corresponding SLD profile is shown in the inset. Since the PBS program did not take X-ray absorption into account, the SLD profile was checked using a model-dependent program, TMLAYER,³⁸ which incorporates X-ray absorption in the calculation of reflectivity curves from SLD profiles. The model reflectivity data generated by the TMLAYER program, using the SLD profile found with PBS, matched the measured reflectivity data. It is evident from the SLD profile that the gold–air interface is not sharp but extends from $z = 0$ to $z = 8–10$ Å. This is an indication of the “roughness” of the interface and will be discussed later with respect to the neutron reflectivity data.

For use with neutron reflectivity data, the SLD values of the gold and chromium were adjusted to their corresponding neutron values and the SLD profile was reversed so that $z = 0$ defined the edge of the silicon–chromium interface, rather than the edge of the gold–air interface. This adjusted profile was then used as a starting point for the neutron SLD profile of the chromium and gold regions when fitting the neutron reflectivity data.

Octadecanethiol/dDMPC HBMs. Figure 3 shows the neutron reflectivity data obtained from two different octadecanethiol/dDMPC HBMs in D₂O solution in the presence of melittin. Since data from this HBM in the absence of melittin are not available, these data were not used to evaluate the effect of melittin on the octadecanethiol/dDMPC HBM. However, the data, obtained from two octadecanethiol/dDMPC HBMs prepared 5 months apart (sample no. 1 and sample no. 2), do allow assessment of the reproducibility of the bilayer. Other than having been prepared on the same gold-coated silicon substrate, the two HBMs did not have any common components. The HBM of sample no. 1 was completely removed, and new octadecanethiol and phospholipid layers were added to make sample no. 2. Despite the slightly different treatment of the octadecanethiol layer, as outlined in the Materials and Methods section, it is evident from Figure

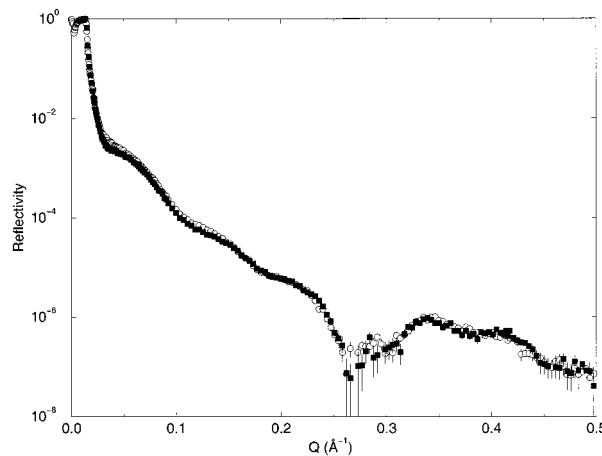


Figure 3. Neutron reflectivity data from octadecanethiol/dDMPC HBMs in D₂O solution containing melittin. Sample no. 1 (○) was prepared 5 months earlier than sample no. 2 (■). Both samples were formed on the same gold-coated silicon substrate.

3 that the two samples are essentially identical. Therefore, it can be concluded that the sample preparation method results in HBMs that are reproducible at length scales that can be measured using neutron reflectometry.

A notable feature of the data in Figure 3 is that the reflected intensity extends down to 10^{-7} and out to $Q = 0.5$ Å⁻¹. This large range of data provides an opportunity for achieving unprecedented structural detail at very high resolution in the z -axis direction. However, this also poses the challenge of how to achieve unbiased fits to the data. If a model-dependent method were used, it would be difficult to build a model with sufficient structural detail to obtain good fits to the data over the entire Q range. Even if such a model were found, the requisite structural detail would result in a large number of adjustable parameters. Therefore, the “model-independent” fitting program, PBS, which is based on a purely mathematical solution, was used as described earlier.

A number of PBS fits, in which only the gold and chromium regions of the neutron SLD profiles were constrained to be the same, were made to the data from both sample no. 1 and sample no. 2. This fitting procedure resulted in a family of neutron SLD profiles, which represent equally good fits to the data in each case. The resultant SLD profiles are shown for the sample no. 2 data in Figure 4, with the PBS fits to the data shown in the inset. The SLD profiles are quite consistent. Since all of the resultant SLD profiles sit on top of each other in the interfacial region between the gold (Au) and the alkanethiol sulfur (S) layers, it is evident that both the SLD and the position of this interface are known unambiguously. The same conclusion can be drawn for the SLD and the position of the interface between the alkanethiol (CH₂) and dDMPC (CD₂) layers. However, the exact shape of the SLD profile at the CD₂–lipid headgroup interface and at the lipid headgroup–D₂O interface is more ambiguous, since there is a larger variation among the resultant SLD profiles in these regions. It is also evident that the shape of the CH₂ region is asymmetric. A homogeneous CH₂ layer should have a constant SLD value for 75 Å $\leq z \leq 95$ Å. However, the SLD values for all curves increase as a function of z in this region, suggesting a “mixing” of the CH₂ and CD₂ regions, defined by the CH₂/CD₂ label in the figure. Yet, if the thickness of the CH₂ layer is taken to be the distance between the centers of the gold–alkanethiol and the alkanethiol–dDMPC

(38) Ankner, J. F.; Majkrzak, C. F. In *SPIE Conference Proceedings*; Majkrzak, C. F., Wood, J. L., Eds.; SPIE: Bellingham, WA, 1992; Vol. 1738.

(39) Collins, R. W.; Allara, D. L.; Kim, Y.-K.; Lu, Y.; Shi, J. In *Characterization of Organic Thin Films*; Ulman, A., Ed.; Butterworth-Heinemann: Boston, MA, 1995; p 48.

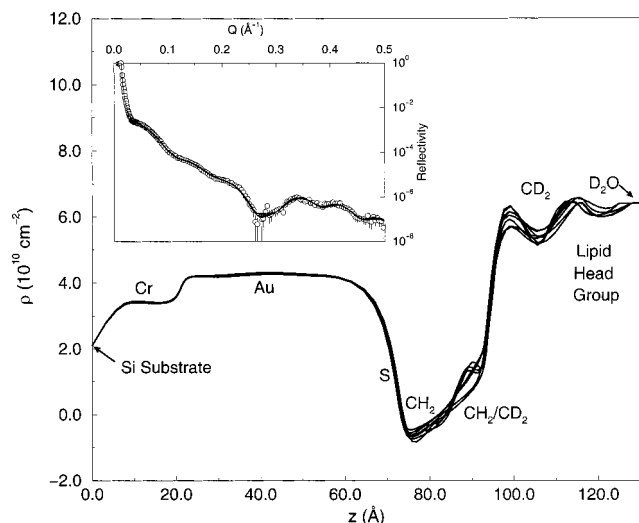


Figure 4. Family of neutron SLD profiles obtained from PBS fits to the data from octadecanethiol/dDMPC HBM sample no. 2. The sample no. 2 reflectivity data are shown in the inset, along with the PBS fits corresponding to the SLD profiles. Each SLD profile represents an equally good fit to the reflectivity data, using the criteria described in the text.

interfaces, it agrees with the expected value^{6,39} of 23 ± 1 Å for octadecanethiol.

This apparent paradox can be explained by considering the effect of the roughness of the gold-coated substrate on the data and subsequent fitted SLD profiles. The fitted SLD profiles for both sample no. 1 (orange shaded area) and sample no. 2 (purple shaded area) are shown in Figure 5. The shaded regions define the boundaries of all of the fits made to each data set. Except for a relatively small constant offset for $80 \leq z \leq 100$, the profiles are nearly identical for both HBMs, in agreement with the reflectivity data of Figure 3. The solid green line in Figure 5 is the SLD profile generated from the results of a molecular dynamics (MD) simulation⁴⁰ of an octadecanethiol/DPPC HBM, where the DPPC leaflet is in the fluid phase. This simulation containing DPPC only approximates the experimental system, since it includes two 16-carbon acyl chains, while the measured HBM contained DMPC, with two 14-carbon acyl chains. Therefore, the lipid acyl chain region (CD_2) of the fitted SLD profiles should be about 3 Å thinner than that of the simulated SLD profile. Given this, it is evident that the simulated SLD profile resembles those obtained from the data. However, the gold-alkanethiol and alkanethiol-dDMPC interfaces of the simulated profile are much sharper.

The X-ray reflectivity data from the gold-coated silicon substrate indicate that the gold surface is not a discrete interface but extends over a distance of 8–10 Å normal to the surface. To simulate this roughness at the gold surface, the simulation-derived SLD profile was convoluted with a Gaussian function with a standard deviation of 4 Å. The resultant “rough” SLD profile is shown as the solid black line in Figure 5. Notice that the “rough” simulated SLD profile now matches the data quite well at the gold-alkanethiol and alkanethiol-dDMPC interfaces. However, it is a poor representation of the measured SLD profiles for the dDMPC leaflet. In particular, the “rough” simulated SLD profile shows much less structure than the measured profiles for $z > 95$ Å. In fact, the original simulated profile that does not take the surface roughness

into account (solid green line in Figure 5) is a better representation of the experimental SLD profiles for the dDMPC leaflet. This can be explained if the rigid alkanethiol leaflet adapts a roughness conformal to that at the gold-alkanethiol interface, while the more fluid dDMPC leaflet effectively anneals, resulting in a smoother surface and sharper transitions between the acyl layer (CD_2) and the headgroup, as well as between the headgroup layer and the bulk water. This is illustrated in Figure 6, where a molecular representation of the simulated octadecanethiol/DPPC HBM⁴⁰ is superimposed on the fitted SLD profiles obtained from the neutron reflectivity data.

THEO-C₁₈/dDMPC HBMs. Data were obtained for the THEO-C₁₈/dDMPC hybrid bilayers in D₂O in both the presence and absence of melittin, and the resultant SLD profiles were directly compared. These SLD profiles for the HBMs in the presence (gray shaded area) and absence (black shaded area) of melittin in the solution are shown in Figure 7. For clarity, the gold and chromium layers are not shown. The reflectivity data, from which these profiles were obtained, are plotted in the inset. In this case, the reflected intensities approach 10^{-8} and extend out to $Q = 0.7 \text{ Å}^{-1}$. As described earlier, the SLD profiles represent a family of profiles that result from multiple iterative fits to the data using the PBS program. The profiles shown represent the best fits in which the gold and chromium layers were constrained to be the same in both data sets. It is evident that the changes in the reflectivity curves, while large at certain Q values, are distributed over the range of Q values measured. On the other hand, changes in the resultant SLD profiles are highly localized to the region $z \geq 110$ Å. Note that the shapes of the SLD profiles at the gold-ethylene oxide and CH_2 - CD_2 interfaces are again characteristic of the roughness of the gold surface, as discussed above for the octadecanethiol/dDMPC data. Compared to the case of the octadecanethiol/dDMPC HBM, the CH_2 - CD_2 interface in this bilayer is described by a broader line, indicating larger variation within the family of curves and greater ambiguity in knowing the location of that interface. The combined thickness of the ethylene oxide and alkanethiol regions, when measured from the center of the gold-ethylene oxide interface to the center of the alkanethiol-dDMPC interface, agrees with the expected value³² of 41–43 Å for the HBM in the absence of melittin. The magnitudes of the SLD values in the dDMPC acyl chain (CD_2) and lipid headgroup regions in the absence of melittin are somewhat lower than those predicted from the MD simulation of Tarek et al.,⁴⁰ possibly because the phospholipid layer is not as dense in the sample as in the simulated HBM.

One conclusion that can be drawn from the SLD profile for the THEO-C₁₈/dDMPC HBM in the absence of melittin is that the ethylene oxide region ($70 \text{ Å} \leq z \leq 90 \text{ Å}$) is not hydrated. The average SLD for this region (see Table 1) is close to $0.5 \times 10^{10} \text{ cm}^{-2}$, the value expected for a homogeneous, unhydrated ethylene oxide layer, based strictly on its chemical composition and mass density. Since the HBM was in contact with D₂O solution, the presence of D₂O in the ethylene oxide region would have resulted in a higher SLD in the corresponding part of the SLD profile. This result corroborates the IR measurements,³² indicating that the THEO-C₁₈ monolayer is highly ordered in air. Apparently, this leaflet retains its highly ordered configuration in the hydrated THEO-C₁₈/dDMPC HBM. Additionally, it is evident from the SLD profiles in Figure 7 that the presence of melittin does not change the hydration of the ethylene oxide region. Thus, there is no evidence from these data that melittin has had the effect

(40) Tarek, M.; Tu, K.; Klein, J. L.; Tobias, D. J. *Biophys. J.* **1999**, *77*, 964.

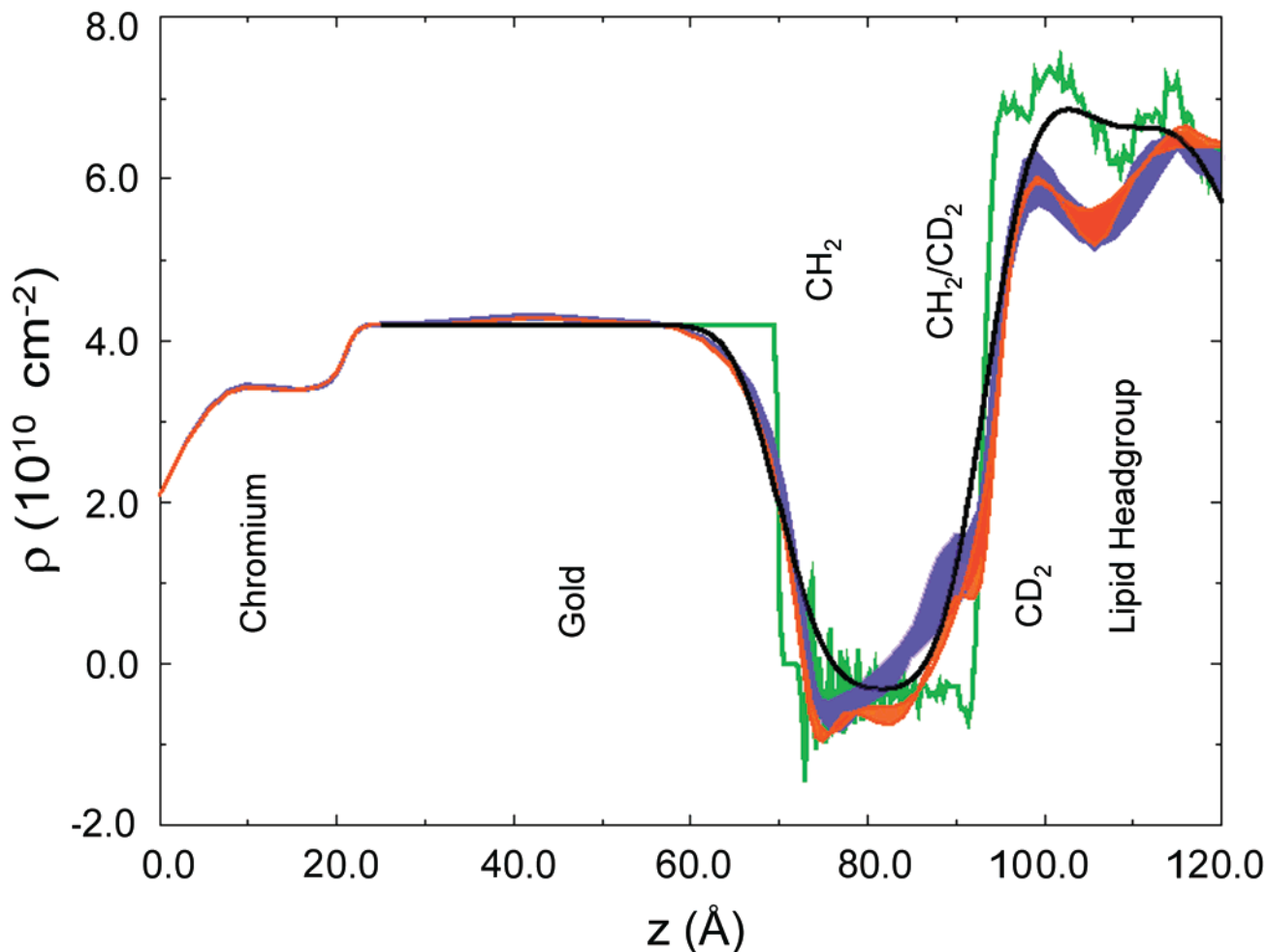


Figure 5. Family of neutron SLD profiles obtained from PBS fits to the data from octadecanethiol/dDMPC HBM sample no. 1 (orange shaded area) and sample no. 2 (purple shaded area). The solid green line is the SLD profile calculated from a molecular dynamics simulation⁴⁰ of a fully hydrated octadecanethiol/DPPC bilayer, where the DPPC leaflet is in the fluid phase. Note that the lipid acyl chain region (CD_2) of the fitted SLD profiles with dDMPC should be about 3 Å smaller than that of the simulated SLD profile with DPPC. The solid black line is the simulation-derived SLD profile convoluted with a Gaussian function with a standard deviation of 4 Å, to simulate the roughness at the gold surface that was observed in the X-ray reflectivity data.

of opening up a discrete aqueous channel through the membrane.

To determine if the location of melittin can be ascertained in the THEO- C_{18} /dDMPC HBMs, SLD values were calculated for the HBMs with and without melittin either from the chemical composition of the various different regions in the SLD profiles or from the MD simulation of Tarek et al.⁴⁰ These calculated values are listed along with the measured values in Tables 1 and 2. The specific assumptions used in these calculations are noted in the tables.

The effect of the addition of melittin on the alkyl chain region of the HBM is ambiguous. This is partly because of the wide range of SLD values that can be assigned to the CD_2 layer in the presence and absence of melittin. In addition, the decrease in the SLD of this layer that would be predicted due to the presence of melittin could be offset by the presence of D_2O in the layer. On the basis of the results from X-ray and neutron diffraction experiments on ordered stacks of DOPC bilayers containing deuterated melittin, Bradshaw et al.⁴¹ reported a continuous band of water (or at least protons) across the bilayer. Association of water with melittin in the interior of the acyl chain region appears to be corroborated by molecular dynamics

simulations of a single melittin molecule in a DMPC bilayer.⁴² Assuming 50 lipids per melittin molecule in the layer, the SLD in the dDMPC acyl chain layer is expected to decrease from a value of $7.4 \times 10^{10} \text{ cm}^{-2}$, as given in Table 1, to $7.2 \times 10^{10} \text{ cm}^{-2}$, as given in Table 2. This certainly falls within the range of the observed changes. However, the SLD of D_2O , $6.4 \times 10^{10} \text{ cm}^{-2}$, is close to both of these SLD values, so it would be difficult to detect the presence of D_2O in the dDMPC acyl chain region.

On the other hand, the change in the SLD value in the lipid headgroup region upon the addition of melittin is seen distinctly (Figure 7 and Tables 1 and 2). If all of the added melittin associates with the lipid, the SLD is expected to decrease in the headgroup region from $6.0 \times 10^{10} \text{ cm}^{-2}$, as given in Table 1, to $5.6 \times 10^{10} \text{ cm}^{-2}$ or $5.8 \times 10^{10} \text{ cm}^{-2}$, depending upon the orientation of melittin, as given in Table 2. This represents a change in SLD of 3–6%, whereas the observed decrease is as much as a factor of 2 in the presence of melittin. The magnitude of this change strongly suggests that water, or in this case D_2O , is displaced from the headgroup region, lowering the SLD considerably. This water displacement would presumably take place in conjunction with a rearrangement of the lipid molecules to accommodate the volume occupied by melittin. Bradshaw et al.⁴¹ also report the apparent

(41) Bradshaw, J. P.; Dempsey, C. E.; Watts, A. *Mol. Membr. Biol.* **1994**, *11*, 79.

(42) Bernèche, S.; Mafalda, N.; Benoit, R. *Biophys. J.* **1998**, *75*, 1603.

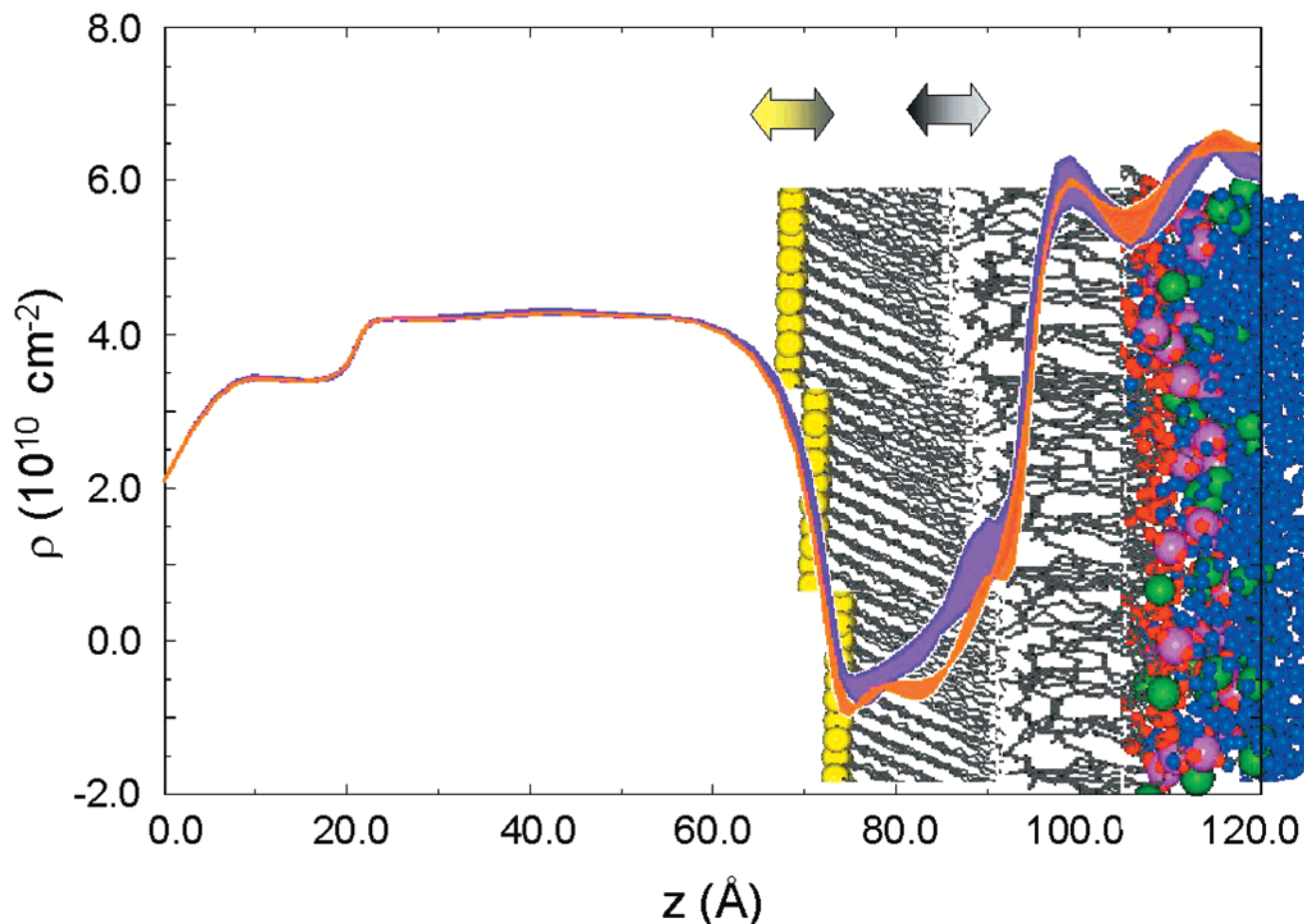


Figure 6. Molecular representation of the octadecanethiol/DPPC HBM from the molecular dynamics simulation of Tarek et al.⁴⁰ superimposed on the fitted neutron SLD profiles for octadecanethiol/dDMPC HBM sample no. 1 (orange shaded area) and sample no. 2 (purple shaded area). The roughness in the octadecanethiol leaflet is conformal with that of the gold surface. However, the proximal phospholipid leaflet is in the more disordered fluid phase and anneals, smoothing out the roughness present in the distal leaflet of the bilayer.

displacement of water by melittin in the hydrated region of DOPC lipid multilayers.

Additional neutron reflectometry measurements can be performed on the same THEO-C₁₈/DMPC HBMs, but with a different combination of hydrogenated and deuterated components, to increase the sensitivity of the technique to the presence of melittin and water in the DMPC acyl chain and lipid headgroup regions. However, it may prove difficult or impractical to quantify the contributions of melittin and water separately in the acyl chain region, since perdeuterated peptide and D₂O have similar SLDs, as do CH₂ and H₂O. The experimental parameters chosen for this study, that is, hydrogenated THEO-C₁₈, d₅₄-DMPC, and nondeuterated melittin in D₂O, do provide sufficient contrast to verify that the THEO-C₁₈ region is highly ordered and to show that the neutron reflectometry technique is sensitive to structural changes in the HBM due to the presence of melittin. Since this HBM does not have the desired biomimetic character, more detailed studies with different deuterated components are being deferred to HBMs formed using alternate tethering chemistries.

A striking feature of the SLD profiles in Figure 7 is the apparent change in the location of the CH₂-CD₂ interface by as much as 3 Å in the presence of melittin. This change can occur if the alkane chains of the THEO-C₁₈ have gotten longer, presumably by a decrease in the tilt angle. This is consistent with the lower SLD values obtained in both the alkane chain (CH₂) region and the mixed CH₂/CD₂

region, in the presence of melittin (gray shaded area for the range 90 Å ≤ z ≤ 110 Å in Figure 7). The SLD is defined as a scattering length per unit volume. Thus, a change in SLD in a given region could represent either a change in chemical composition of that region or a change in the volume occupied by the components or both. A decrease in the SLD is expected in these regions if the volume occupied by the alkane chains increases. However, an increase in SLD would be expected in the presence of melittin, or melittin and water (D₂O), since the SLD values of both melittin and D₂O are significantly larger than that of CH₂.

The recent X-ray and neutron diffraction results⁴¹ from deuterated melittin in ordered stacks of DOPC bilayers suggest that melittin lies in the phospholipid interface region and penetrates to near the center of the bilayer. The degree of penetration was reported to be enhanced by protonation of the N-terminus residues. Results from the MD simulations of a single melittin molecule in a DMPC bilayer⁴² also suggest that melittin is oriented with most of its α-helix lying parallel with the membrane plane, in the headgroup region, while the N terminus of the peptide extends to the center of the bilayer. Energetics calculations suggest that electrostatic interactions between the polar moieties of the melittin α-helix and the interfacial polar headgroup prevent melittin from inserting any deeper into the bilayer. The molecular dynamics simulation⁴² results also suggest that melittin has the effect of deforming the bilayer by causing curvature of the bilayer

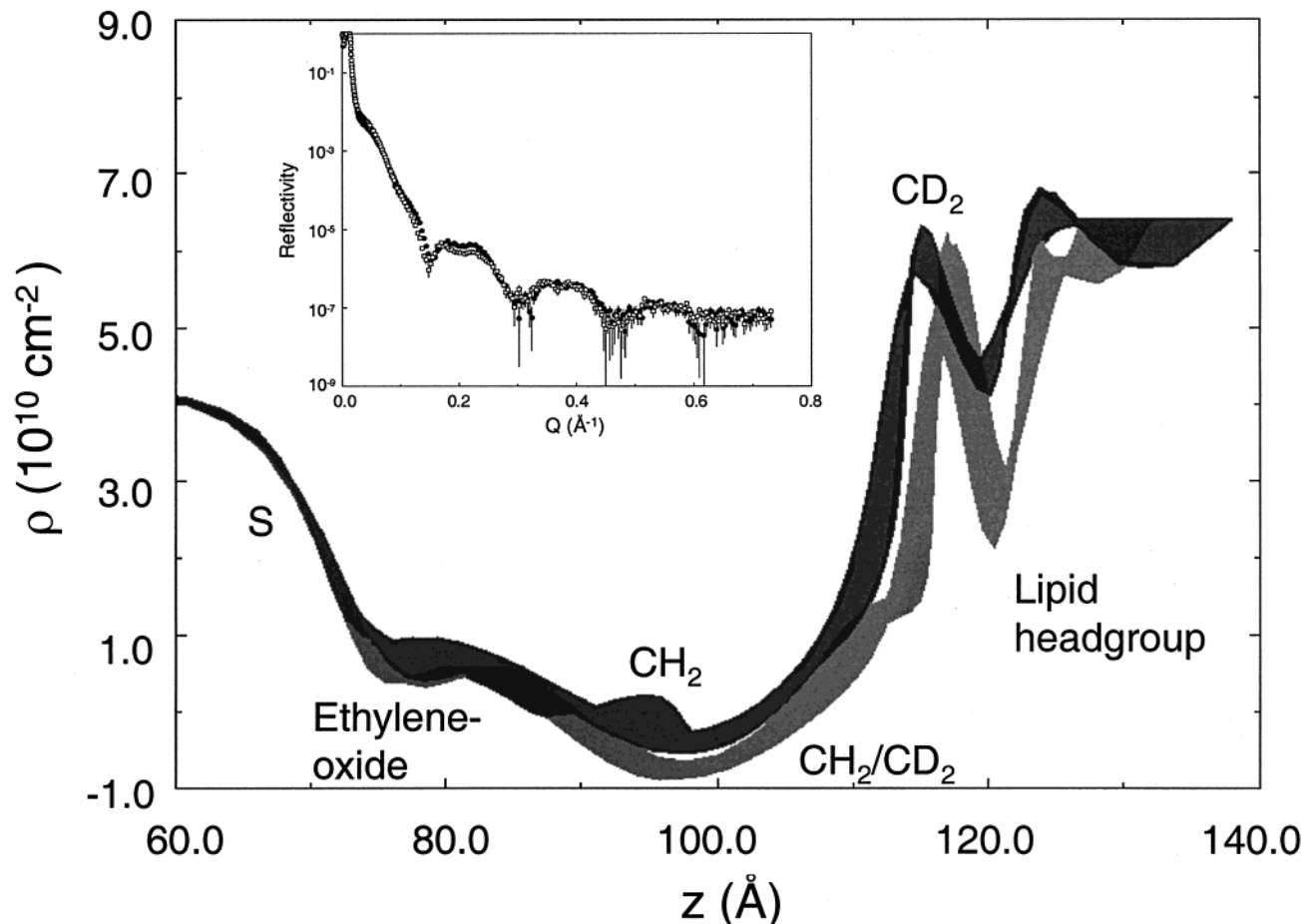


Figure 7. Boundaries of the families of PBS-fitted SLD profiles obtained from the neutron reflectivity data for THEO-C₁₈/dDMPC HBMs in D₂O solution with (gray shaded area) and without (dark gray shaded area outlined in black) melittin. The chromium and gold regions are not shown in the SLD profiles for clarity, since they are essentially identical to the same regions in the profiles of Figure 4. The neutron reflectivity data for THEO-C₁₈/dDMPC HBMs in D₂O solution with (□) and without (●) melittin are shown in the inset.

Table 1. SLD Values for the Thiahexa(ethylene oxide) C₁₈/dDMPC HBM without Melittin

approximate <i>z</i> range (Å)	nominal composition	expected SLD ^a (10 ¹⁰ cm ⁻²)	measured SLD (10 ¹⁰ cm ⁻²)
0–20	chromium	3.0	3.5
20–65	gold	4.5	4.1–4.3
65–85	ethylene oxide	0.5	0.35–0.65
85–100	CH ₂	–0.4	–0.85 to –0.35 ^c
100–110	mixed CH ₂ /CD ₂		–0.35–5.8
110–120	CD ₂	7.4 ^b	5.8–6.0
120–130+	lipid headgroup	6.0 ^b	4.3–4.5

^a SLD values were determined directly from the chemical composition of the material, unless otherwise noted. ^b SLD values were determined from Tarek et al.⁴⁰ assuming no water in the CD₂ region and 1 lipid per 10.5 water molecules in the lipid headgroup region. The maximum value was chosen in the CD₂ region, and the minimum value was chosen in the lipid headgroup region. ^c Range of SLD values was calculated using all SLD profiles (black and gray) shown in Figure 7.

in the vicinity of the melittin and reducing the hydrophobic core by 30%. As the simulation progressed, the results suggested increasing disorder in the proximal leaflet of the bilayer (where melittin is located) and increasing order in the distal leaflet of the bilayer. The net effect is that the acyl chains of the distal layer are more extended due to the presence of melittin. The reflectivity results presented here show a distinct change in the bilayer that could indicate a shift of up to 3 Å in the position of the interface between the leaflets of the bilayer.

Table 2. SLD Values for the Thiahexa(ethylene oxide) C₁₈/dDMPC HBM with Melittin

approximate <i>z</i> range (Å)	nominal composition	expected SLD ^a (10 ¹⁰ cm ⁻²)	measured SLD (10 ¹⁰ cm ⁻²)
0–20	chromium	3.0	3.5
20–65	gold	4.5	4.1–4.3
65–85	ethylene oxide	0.5	0.35–0.65
85–100	CH ₂	–0.4	–0.85 to –0.35 ^c
100–113	mixed CH ₂ /CD ₂		–0.35–5.8
113–123	CD ₂ + melittin	7.2 ^b	4.5–6.1
123–130+	lipid headgroup + melittin	5.6–5.8 ^b	2.1–3.2

^a SLD values were determined directly from the chemical composition of the material, unless otherwise noted. ^b SLD values were determined starting from the values in Table 1, assuming a melittin concentration equivalent to 1 melittin per 50 lipid molecules, no water in the CD₂ region, and 1 lipid per 10.5 water molecules in the lipid headgroup region. Localized changes in the lipid density due to the insertion of melittin are not taken into account. The range of values in the lipid headgroup region results from the consideration of melittin oriented both parallel and perpendicular to the plane of the bilayer. Only the perpendicular orientation was considered for the CD₂ region. The SLD for melittin in D₂O was taken to be 3.0 × 10¹⁰ cm⁻², calculated from its amino acid composition, assuming a partial specific volume of 0.73 cm³/g and assuming 80% H → D exchange of all exchangeable H molecules. ^c The range of SLD values was calculated using all SLD profiles (black and gray) shown in Figure 7.

Conclusions

Neutron reflectometry has been used to study structural details in octadecanethiol/dDMPC HBMs and THEO-C₁₈/

dDMPC HBMs and to assess the sensitivity of the technique to the presence of melittin in the THEO-C₁₈/dDMPC HBM. To obtain Angstrom-level information about the structure of these HBMs, improvements in instrumentation and the sample environment were made to allow reflectivity data to be obtained down to 10^{-8} in reflected intensity and out to Q values as high as 0.7 \AA^{-1} . The structures of both HBMs were quantified by comparing the resultant SLD profiles to profiles generated by molecular dynamics simulations⁴⁰ of octadecanethiol/DPPC HBMs. It was found that the octadecanethiol and THEO-C₁₈ leaflets of the HBMs exhibit roughness conformal with that of the gold surface. However, this roughness did not propagate throughout the dDMPC phospholipid leaflet in either HBM. Since the phospholipid is in the fluid state, the dDMPC leaflet is much more disordered than either the octadecanethiol or THEO-C₁₈ leaflets. Therefore, the dDMPC essentially anneals, smoothing out the roughness present in the distal leaflet of the bilayers.

The sensitivity of the reflectometry technique to the presence of melittin was assessed by comparing data for the THEO-C₁₈/dDMPC HBMs in both the presence and absence of melittin. First, it is evident that the ethylene oxide region of the THEO-C₁₈ leaflet is not hydrated with D₂O from the solution and that melittin does not alter the HBM in a way that allows bulk water to penetrate into this region. This not only confirms the surprising results of FTIR experiments³² on dry THEO-C₁₈ monolayers, which indicated a high degree of molecular order in air, but also extends them to THEO-C₁₈ monolayers in HBMs in contact with water. As a result, alternate tethering chemistries, which will hopefully lead to a more biomimetic HBM, are currently being pursued.

The neutron reflectivity experiments clearly show that melittin has the greatest effect on the SLD profiles in the dDMPC headgroup region. In fact, the large change in SLD strongly suggests that D₂O is displaced from this region upon the insertion of melittin. The technique does not appear to be as sensitive to the presence of melittin in the dDMPC acyl chain region. However, the simultaneous presence of D₂O and melittin in this region cannot be ruled out, since the presence of either would not change the SLD of the layer appreciably. The data also indicate that melittin has a significant effect on the THEO-C₁₈ leaflet. The interface between the alkane chains and the dDMPC acyl chains appears to be displaced to higher z values by as much as 3 \AA . This can occur if the length of the alkane chains has increased, presumably through a decrease in tilt angle. This result agrees with those of molecular dynamics simulations of a single melittin molecule in a DMPC bilayer,⁴² which suggest that the presence of melittin not only affects the lipid leaflet in which it is present but also affects the distal leaflet of the bilayer as well. One result of this influence is that the density minimum, which indicates the center of the bilayer, is observed in the simulation to move approximately 2.5 \AA toward the proximal leaflet due to the presence of melittin.

Overall, the results indicate that the neutron reflectometry technique, as used here with improvements in instrumentation and experimental design, now provides enough sensitivity and resolution to warrant a complete study of melittin in HBMs. This would include multiple measurements of the HBM/melittin system with different sets of deuterated components and with different concentrations of melittin in the solution. Furthermore, the experiments should be performed on a more biomimetic HBM that is not tethered with an ethylene oxide moiety.

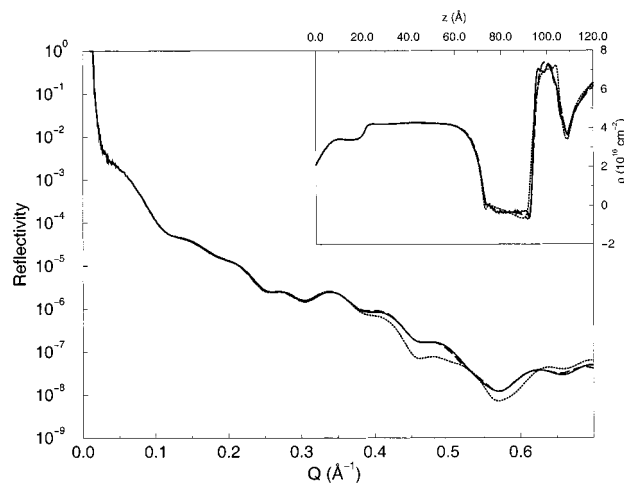


Figure 8. Simulated reflectivity data (—) calculated from a model SLD profile that mimics the expected profile for the octadecanethiol/dDMPC HBM, along with PBS fits to this calculated reflectivity curve for Q values out to 0.3 \AA^{-1} (---, extended out to 0.7 \AA^{-1}) and for Q values out to 0.7 \AA^{-1} (---). The inset shows the model SLD profile (—), along with the profiles obtained from the PBS fits out to 0.3 \AA^{-1} (---) and 0.7 \AA^{-1} (---).

The current experimental method can be further improved by the use of phase-sensitive neutron reflectometry techniques^{43–46} that allow the SLD profile to be obtained by a first-principles inversion without the need to perform multiple fits to the data. In particular, the applicability of the surround variation⁴⁵ phase inversion method has been shown⁴⁷ for the THEO-C₁₈/dDMPC HBM in the absence of melittin. As a result, phase-sensitive neutron reflectometry methods are already being incorporated into current studies of melittin in HBMs with modified tethering chemistries.

Appendix A: Testing the PBS Program

To test the PBS program, simulated reflectivity data were calculated from a model SLD profile (solid line) which mimics the expected profile for the octadecanethiol/dDMPC HBM. Gold and chromium layers were added to the model profile, and a back silicon substrate with a silicon oxide layer was also assumed to be present. The PBS fit to the calculated reflectivity curve for Q values out to 0.3 \AA^{-1} is shown as the dotted line in Figure 8. Although the known SLD values for the chromium and the gold layers were used, and a silicon-oxide layer was assumed to exist on the back silicon substrate, the resultant SLD profile (dotted line in the inset) does not match the original well beyond $z = 70 \text{ \AA}$. If the reflectivity curve is calculated out to $Q = 0.7 \text{ \AA}^{-1}$ directly from this ill-matching SLD profile, as shown by the extended dotted line in Figure 8, it is evident that it differs significantly from the simulated reflectivity curve beyond a Q value of 0.35 \AA^{-1} . On the other hand, if the simulated data are fit to $Q = 0.7 \text{ \AA}^{-1}$ (dashed line in Figure 8), the fitted SLD profile (dashed line in the inset) matches the model profile quite well at all z values, except for the failure to resolve the two small

(43) Majkrzak, C. F.; Berk, N. F. *Phys. Rev. B* **1995**, *52*, 10827.

(44) de Haan, V. O.; van Well, A. A.; Adenwall, S.; Felcher, G. P. *Phys. Rev. B* **1995**, *52*, 10831.

(45) Majkrzak, C. F.; Berk, N. F. *Phys. Rev. B* **1998**, *58*, 15416.

(46) Majkrzak, C. F.; Berk, N. F. *Physica B* **1999**, *267–268*, 168.

(47) Majkrzak, C. F.; Berk, N. F.; Krueger, S.; Dura, J. A.; Tarek, M.; Tobias, D.; Silin, V.; Meuse, C. W.; Woodward, J.; Plant, A. L. *Biophys. J.* **2000**, *79*, 3330–3340.

(48) The specification of commercial products is for clarity only and does not constitute endorsement by NIST.

peaks between $z = 95$ and 105 \AA . Thus, the PBS fitting method does result in a good determination of an actual SLD profile, provided that the reflectivity data are measured out to a high enough Q value, especially when the shape of a portion of the profile, such as the chromium and gold layers, is already known. In a typical experiment, the exact SLD values of the chromium and gold layers as a function of z are not known. Additionally, the exact

composition of the silicon oxide layer on the back substrate is unknown and the data near the background values are noisy. This makes it essential to make multiple PBS fits to the data, using the information for the chromium and gold layers obtained from X-ray reflectivity measurements, to obtain a family of curves which represent the SLD profile of the HBM.

LA001134T